Microelectronic Engineering 110 (2013) 241–245

Contents lists available at SciVerse ScienceDirect

Microelectronic Engineering

journal homepage: www.elsevier.com/locate/mee

Effect of annealing temperature on microstructure and magnetism of FePt/TaO_x bilayer

Guijun Li [a], Chi Wah Leung [b], Ying-Ching Chen [c], Ko-Wei Lin [c,*], An-Cheng Sun [d], Jen-Hwa Hsu [e], Philip W.T. Pong [a,*]

[a] Department of Electrical and Electronic Engineering, The University of Hong Kong, Hong Kong
[b] Department of Applied Physics, Hong Kong Polytechnic University, Hong Kong
[c] Department of Materials Science and Engineering, National Chung Hsing University, Taichung, Taiwan
[d] Department of Chemical Engineering and Materials Science, Yuan Ze University, Taiwan
[e] Department of Physics, National Taiwan University, Taiwan

ARTICLE INFO

Article history:
Available online 26 January 2013

Keywords:
FePt
TaO_x
Annealing temperature
Coercivity

ABSTRACT

The effect of annealing temperatures on the microstructures and magnetism of FePt/TaO_x bilayers was systemically investigated in the range of 25–650 °C. Microstructural characterization reveals that higher annealing temperatures lead to higher ordering parameters and larger grain sizes. High order parameter up to 0.57 was acquired after the sample was annealed at 600 °C. Diffusion was observed from TaO_x layer into FePt layer after annealing at temperature over 550 °C. The out-of-plane coercivity first increased and exhibited a maximum value up of 4.2 kOe after annealing at 550 °C and decreased as the annealing temperature was further increased. The coercivity increase with higher annealing temperature was attributed to the rise of magnetocrystalline anisotropy due to the formation of the ordered fct FePt structures.

1. Introduction

Typical magnetic recording media suffer from superparamagnetic effect when the grain size goes into nanometer scale and could not support recording density over 5T bit/in^2 [1]. Magnetic materials with high magnetocrystalline anisotropy are actively investigated for their high thermal stabilities, including binary alloys such as FePt [2,3] and CoPt [4,5]. Stoichiometric FePt has two phases at room temperature, the soft fcc (face center cubic) phase and the harder fct (face center tetragonal) phase. The fct FePt has large magnetocrystalline anisotropy up to 7×10^7 erg/cm^3 and is considered a promising candidate for the future ultrahigh density recording medium [6–8]. However, fct phase FePt cannot be directly synthesized and it can only be phase transformed from fcc phase FePt. For example fct FePt could firstly be synthesized as fcc phase FePt and then thermally annealed to the fct phase [9].

Since different annealing temperatures and different types of buffer layers under the FePt film would both influence the microstructures and magnetic properties of FePt, a lot of researches have focused on the effect of annealing with different capping layers [10–13]. For example, a 4 nm Cu capping layer was found to raise the coercivity of FePt drastically from 3100 to 6000 Oe [14]. With a single SiO_2 capping layer, annealing at 400 °C was sufficient to transform the fcc phase FePt to fct phase [15]. Meanwhile, TaO_x is an important metal oxide widely used as the capping and buffer layers in multilayered structures [16]. For example, $Ge_2Sb_2Te_5$-TaO_x composited films were found to have the residual stress reduced by 40% compared to pure phase change material $Ge_2Sb_2Te_5$ [17]. However, there is no previous investigation using TaO_x as a capping layer on FePt.

In view of this, we studied the structural and magnetic properties of co-sputtered FePt thin films capped by TaO_x layer sputtered with 15% O_2/Ar gas mixture annealed at different temperatures (up to 650 °C). The microstructures of FePt/TaO_x bilayers were investigated by X-ray diffraction (XRD), transmission electron microscopy (TEM) and X-ray photoelectron spectroscopy (XPS). The magnetic properties were characterized by vibrating sample magnetometer (VSM). As the annealing temperature increased, the growth of grain sizes and the rise of coercivities were observed. An optimized annealing temperature of 550 °C was found to provide the highest coercivity (4.2 kOe) in the out-of-plane direction.

2. Experiments

The FePt films (10 nm) were co-sputtered on SiO_2 substrates using an ultrahigh vacuum magnetron sputtering system with dc power of 70 W for Fe and 34 W for Pt, using 3 sccm Ar with a chamber pressure of 10 mTorr. The 10 nm thick TaO_x capping layer

* Corresponding authors. Tel.: +852 28578491; fax: +852 25598738 (P.W.T. Pong), tel.: +886 4 22851068; fax: +886 4 22857017 (K.-W. Lin).
E-mail addresses: kwlin@dragon.nchu.edu.tw (K.-W. Lin), ppong@eee.hku.hk (P.W.T. Pong).

0167-9317/$ - see front matter © 2013 Elsevier B.V. All rights reserved.
http://dx.doi.org/10.1016/j.mee.2013.01.028

was then deposited by using ion-beam assisted deposition (IBAD) with 0.4 sccm of O_2 and 2.3 sccm of Ar (15% O_2/Ar). Then the samples were annealed in vacuum at different temperatures ranging from 400 to 650 °C for 10 min, with no external magnetic field applied during the process.

The crystallinitiy of the FePt/TaO_x bilayers was investigated by grazing angle X-ray diffraction using a Bruker D8 SSS diffractometer with Cu K_α source. A JEOL JEM-2010 transmission electron microscopy (TEM) system operating at 200 kV was used for the FePt/TaO_x bilayer surface morphology and cross-section characterization. At last, the ferromagnetic properties of the as-deposited and annealed samples were measured with a Lake Shore – 7407 vibrating sample magnetometer (VSM).

3. Results and discussion

To characterize the effect of annealing temperatures on the crystallinity, the FePt/TaO_x bilayers were studied by XRD. The fcc phase FePt has a cubic structure with the lattice constant a the same in all directions. Meanwhile, the fct phase FePt has a tetragonal structure with a shorter lattice constant c than the other axis a, which contributes to the anisotropy of the fct phase. If we have a smaller c/a ratio, the anisotropy of the fct phase FePt is larger. As-deposited FePt/TaO_x bilayer shows fcc phase, with a lattice constant of $a \sim 3.81$ Å as calculated from the (111), (200), and (220) peaks in the XRD diffraction patterns of the 25 °C spectra in Fig. 1. For the bilayer annealed at 400 °C, similar XRD diffraction patterns as those of as-deposited bilayer indicate that there is little fct FePt phase formation after annealing at this temperature. The calculated lattice constant of the fcc phase FePt is increased to ~3.82 Å (larger than fcc phase with lattice constant of 3.816 Å but smaller than the fct phase constant of $a \sim 3.838$ Å), which also indicates the increase of fct phase FePt content in FePt/TaO_x bilayer. Further increasing the annealing temperature to 550 °C leads to higher fct (001) and (110) peaks in FePt/TaO_x bilayer, indicating more fct phase FePt is formed after annealing at this temperature. The ordering parameter [18] of fct phase FePt is calculated using

$$S = \sqrt{\frac{[I_{(110)}/I_{(111)}]_{\text{measured}}}{[I_{(110)}/I_{(111)}]_{S=1}}}$$

where $I_{(110)}$ and $I_{(111)}$ are the intensities of the XRD peaks of fct phase (110) and (111), the numerators are experimentally measured from the samples and the denominators are the calculated results from an ideal sample with the order parameter S of 1. The lattice constants of FePt in the FePt/TaO_x bilayer after annealing at 550 °C are $a \sim 3.86$ Å, $c \sim 3.70$ Å with an ordering parameter of 0.56. Further increasing the annealing temperature to 600 °C increases the ordering parameter to 0.57 with lattice constants of $a \sim 3.85$ Å and $c \sim 3.70$ Å, as calculated by the stronger fct (001), (111), and (110) peaks in the spectra of 600 °C in Fig. 1. However, although annealing at 650 °C provides even smaller c/a ratio with $a \sim 3.88$ Å and $c \sim 3.68$ Å, the appearance of the strong TaO_2 peak inhibits the ordering parameter of FePt to 0.54, which is smaller than those after annealing at 550 °C and 600 °C. The appearance of the strong TaO_2 peak might be due to the high residual stress in FePt [19] due to the annealing at 650 °C which provide sufficient conditions to grow TaO_2 with strong (110) orientation.

The above results are more clearly shown in Fig. 2, where the ordering parameter of the fct phase FePt is depicted. Further increasing the annealing temperature to 650 °C leads to an even lower ordering parameter of 0.54. The above ordering parameter with different annealing temperatures further demonstrates that increasing the annealing temperature to higher than 600 °C leads to less ordered state FePt, which might be due to the strong interlayer diffusion as confirmed by the XPS results below.

To further investigate the microstructure of FePt/TaO_x bilayers after annealing at different temperatures, high resolution TEM (HRTEM) characterization was performed and the results are shown in Fig. 3. The as-deposited FePt/TaO_x bilayer shows separated grains in the bright field image in Fig. 3(a), with sizes ranging from 8 nm to 10 nm. The dark field image of the as-deposited sample (Fig. 3(b)) shows similar size distribution between 8 and 11 nm for the grains with (111) orientation. The electron diffraction pattern of the as-deposited sample is given in Fig. 3(c), where the diffraction rings of (111), (200), (220), and (222) planes of fcc phase FePt are shown. The FePt/TaO_x bilayer, after annealing at 400 °C for 10 min, shows grain structure with a size distribution ranging from 9 to 12 nm in Fig. 3(d), which is larger than that of the as-deposited sample. The dark field image (Fig. 3(e)) shows identical size distribution between 9 and 12 nm for the grains with (111) orientation. Fcc phase (111), (200), (220), and (311) peaks are observed in the electron diffraction patterns in Fig. 3(f), indicating little fct phase FePt was formed after annealing at 400 °C for 10 min which agrees with the XRD results in Fig. 1. Increasing the annealing temperature to 500 °C leads to larger grain sizes ranging from 10 to 14 nm shown in Fig. 3(g). This size distribution of the grains in the (111) orientation is also observed in the dark field image in Fig. 3(h). This indicates that with higher annealing temperature, the grains can obtain more energy to grow into larger grains. Compared to the sample annealed at 400 °C, more fct phase peaks are observed, including fct phase (001) and (002) planes as shown in Fig. 3(i). This indicates that increasing the annealing temperature from 400 °C to 550 °C would bring in more FePt, which agrees

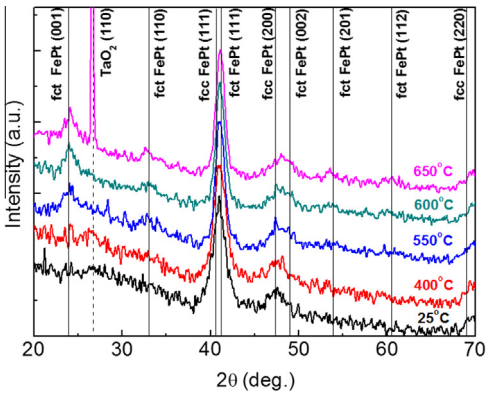

Fig. 1. XRD diffraction patterns of FePt/TaO_x after annealing at different temperatures: as-deposited non-annealing (25 °C), 400 °C, 550 °C, 600 °C, and 650 °C. The standard XRD peak locations are set according to the JCPDS cards.

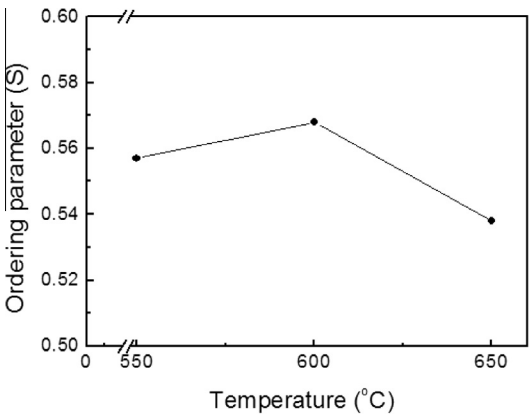

Fig. 2. Ordering parameter of FePt/TaO_x bilayer after annealing at different temperatures: 550 °C, 600 °C and 650 °C.

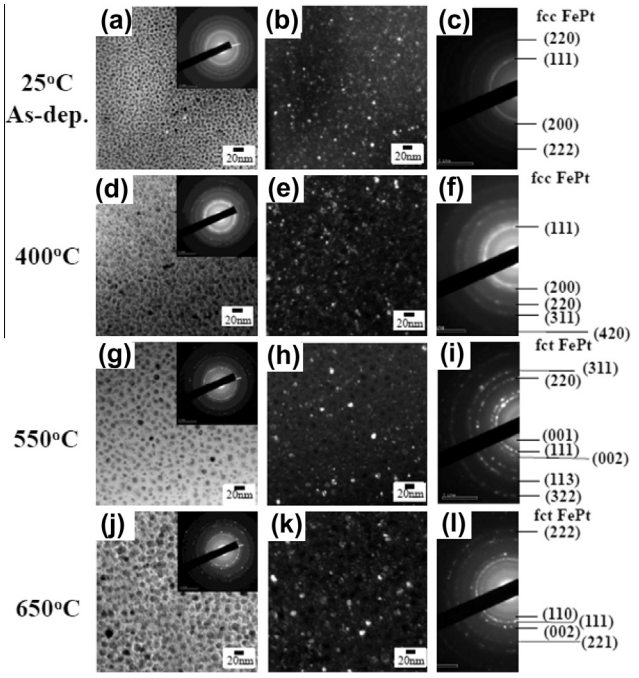

Fig. 3. HRTEM images of FePt/TaO_x bilayers after annealing at different temperatures. Bright field TEM images, dark field TEM images, and electron diffraction patterns are shown as the left, middle, and right images of each row, respectively.

with the increase of ordering parameter in Fig. 2. Further increasing the annealing temperature to 650 °C leads to even wider and larger size distribution, ranging from 12 nm to 20 nm as shown in the bright field TEM image in Fig. 3(j). Large grains with size around 20 nm at (111) orientation are also observed in the dark field image in Fig. 3(k). This indicates that annealing at this temperature can provide energy for FePt to grow into larger size. The electron diffraction patterns of fct phase (110), (111), (002), (221) and (222) planes are found in Fig. 3(l) indicating large content fct FePt formed after annealing at this temperature. The plan view TEM results indicate that as the annealing temperature is increased, the grain size of FePt/TaO_x bilayer is also increased. The electron diffraction results also indicate that as the annealing temperature is increased, more fct phase FePt are formed, which agrees with the XRD results in Fig. 1.

In order to investigate the potential diffusion at the FePt/TaO_x interface, cross-section TEM was performed and the images are shown in Fig. 4. The as-deposited FePt/TaO_x bilayer (25 °C) exhibits

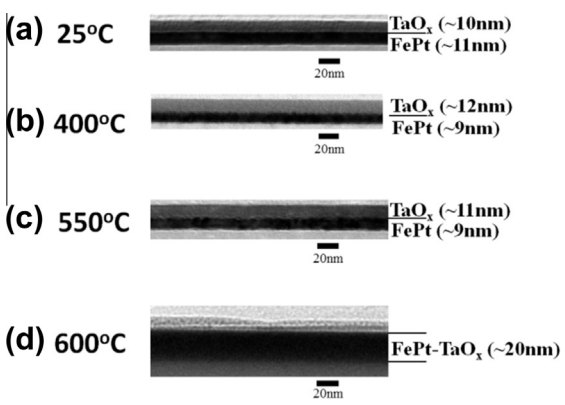

Fig. 4. TEM cross-sectional images of FePt/TaO_x bilayers after annealing at different temperatures: as-deposited (25 °C), 400 °C, 550 °C and 600 °C.

a sharp and clear interface between the FePt and TaO_x layers indicating that there is no diffusion in the as-deposited layers. The TaO_x and FePt layers are measured to be 9.6 nm and 11 nm, respectively, closely matching the designed layer thicknesses (10 nm FePt and 10 nm TaO_x) in Fig. 4(a). After annealing at 400 °C, the interface between TaO_x and FePt is still sharp as shown in Fig. 4(b), indicating no obvious diffusion after annealing at this temperature. Increasing the annealing temperature to 550 °C leads to diffusion between the FePt and TaO_x layers, as proved by the graded FePt/TaO_x interface in Fig. 4(c). This indicates that as the annealing temperature increases, the grains receive enough energy to migrate. Further increasing the annealing temperature to 600 °C leads to more diffusion at the TaO_x and FePt interfaces, and the two layers are almost mixed together as shown in the cross-section image of FePt/TaO_x in Fig. 4(d). This indicates that as the annealing temperature further increases, the grains become even more prone to diffusion. The above results indicate that as the annealing temperature is increased, no diffusion between the FePt and TaO_x layers initially but then slight diffusion starts after annealing at 550 °C for 10 min, and strong diffusion occurs after annealing at 600 °C.

The diffusion between the TaO_x and FePt layers after annealing at 550 °C and 600 °C is also investigated by the XPS depth profiling, and the results are shown in Fig. 5. The TaO_x, FePt, and SiO_2 were etched by XPS sequentially, and the element distribution was measured as a function of sputter time in Fig. 5. The XPS profile of FePt/TaO_x sample annealed at 550 °C is shown in Fig. 5(a). Although there is a sharp transition given by the Fe and Pt distribution starting at 0.6 min in Fig. 5(a), there is a Ta element distribution from 0.6 to 0.9 min, indicating the TaO_x already diffuses into FePt after annealing at 550 °C. Oxygen can also be observed in the FePt layer, which further demonstrates the diffusion from TaO_x into FePt layer. Further increasing the annealing temperature to 650 °C leads to stronger diffusion between the FePt and TaO_x layers. This is supported by the presence of Fe and Pt in the TaO_x layer from 0.3 min to 0.4 min as shown in Fig. 5(b). Ta and O are also present in the FePt layer, similar to the diffusion in Fig. 5(a). Thus the XPS depth profile demonstrates that TaO_x diffuses into FePt after annealing at temperatures higher than 550 °C. The diffusion from TaO_x not only influences the microstructures of the FePt/TaO_x bilayer, it can also influence the magnetic properties of the bilayers.

The XPS binding energy of Ta is displayed in Fig. 6. The peaks of TaO_x layer with energy around 27 eV for both samples after annealing at 550 °C (Fig. 6(a)) and 650 °C (Fig. 6(b)) prove the presence of Ta_2O_5 in the TaO_x layer. It should be pointed out that Ta_2O_5 has a lattice constant of 0.389 nm [20], which is quite similar to the *a*-axis parameter of FePt. As calculated from the XRD patterns in Fig. 1, the lattice constant had a trend that as the annealing temperature is increased, the *a*-axis of FePt started to grow from 0.381 nm to 0.388 nm as shown in Table 1. The underlying FePt layer tended to approach to (001) lattice constant as the capping Ta_2O_5 layer. Thus we can infer that the TaO_x capping layer influences the FePt crystal structure. As the annealing temperature is increased, the Fe and Pt atoms have more energy to rearrange according to the capping TaO_x layer crystal structure, which is quite similar to the other observations where the lattice constants of FePt strongly rely on the underlayers [21–23]. So as the annealing temperature is increased, the *a*-axis of FePt is closer to the Ta_2O_5 (001) *d* spacing. The increase of *a*-axis would further increase the anisotropy of the FePt, which might also increase the coercivities of FePt as discussed below.

To investigate the magnetic properties of FePt, hysteresis loops were measured for FePt/TaO_x bilayers with different annealing temperatures. The out-of-plane coercivities with different annealing temperatures are given in Fig. 7. The as-deposited FePt/TaO_x shows soft magnetic behavior as evidenced by the small out-of-plane coercivity of Hc ~ 60 Oe. This agrees with the XRD

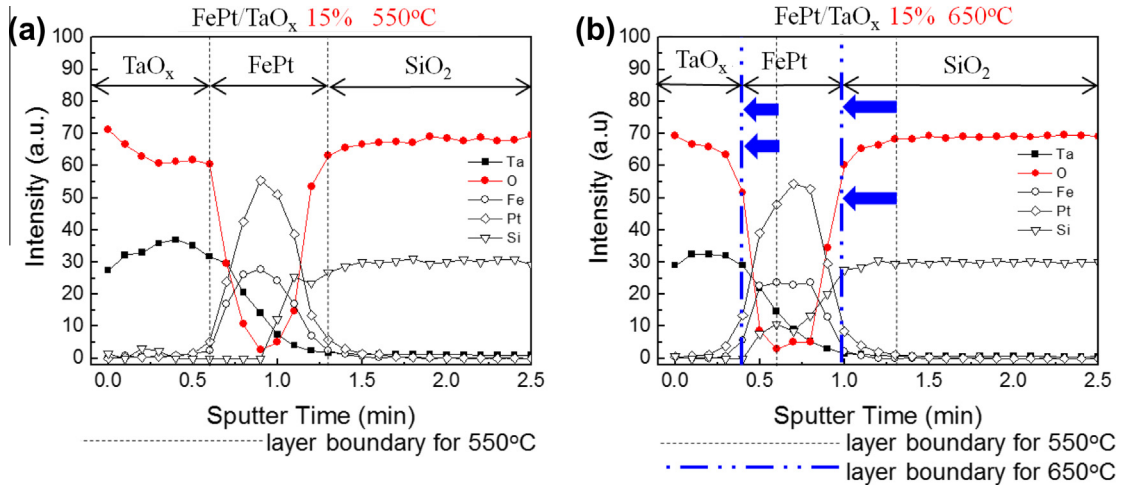

Fig. 5. XPS depth profile of FePt/TaO_x bilayers after annealing at different temperature: 550 °C (a) and 650 °C (b).

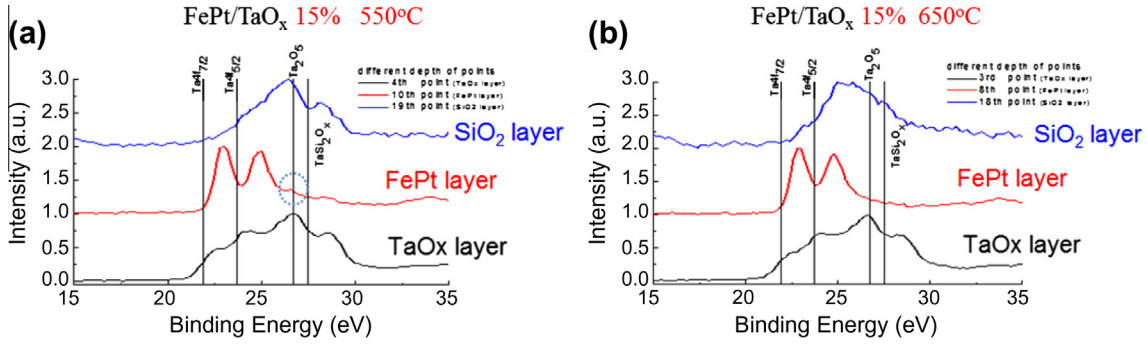

Fig. 6. Binding energy of Ta in FePt/TaO_x bilayers after annealing at different temperatures: 550 °C (a) and 650 °C (b).

Table 1
The relation of lattice constant of FePt and annealing temperature.

Temperature		25 °C (As-dep)	400 °C	550 °C	600 °C	650 °C
Lattice Constant (Å)	*a* (Å)	3.81	3.82	3.86	3.85	3.88
	c (Å)	–	–	3.70	3.70	3.68

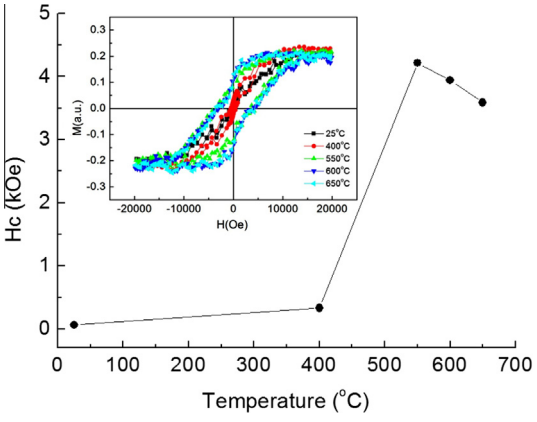

Fig. 7. Coercivity of FePt/TaO_x bilayer after annealing at different temperatures in the out-of-plane directions: as-deposited (25 °C), 400 °C, 550 °C, 600 °C and 650 °C. The corresponding magnetic hysteresis loops are given in the inset.

results that the as-deposited FePt are fcc phase. The FePt/TaO_x bilayer after annealing at 400 °C is still not highly ordered FePt, as proved by the out-of-plane coercivity of 330 Oe. Meanwhile, the increase of the coercivity indicates that there is fct phase FePt formation after annealing at 400 °C, which agrees with the XRD results in Fig. 1. As the annealing temperature is increased to 550 °C, the coercivity rises to 4.2 kOe for the out-of-plane direction. The fct phase FePt becomes dominant after annealing at this temperature. However, annealing at 600 °C decreases the out-of-plane coercivity to 3.9 kOe, indicating that the *c*-axis orientation and the order of FePt are inhibited. Similar to annealing at 600 °C, the FePt/TaO_x bilayer after annealing at 650 °C exhibits decrease of the out-of-plane coercivity to 3.6 kOe. The highest coercivity in the out-of-plane direction is not found in the highest annealing temperature for FePt/TaO_x, indicating that annealing with temperatures higher than 550 °C does not provide a more favourable condition for large out-of-plane coercivity, which also agrees with the XRD results in Fig. 1 and the ordering parameter in Fig. 2. A suitable annealing temperature of 550 °C is critical for FePt capped TaO_x to obtain highest coercivity in the out-of-plane direction.

4. Conclusion

The effect of annealing temperature on the microstructural and magnetic properties of a FePt/TaO_x bilayer was investigated. As the annealing temperatures increased from the as-deposited state (25 °C) to 600 °C, more fct phase FePt was transformed from the fcc phase FePt, as indicated from the XRD diffraction patterns and the ordering parameter; however, further increasing the annealing temperature to 650 °C led to a less ordered state,

indicating less fct phase was formed as compared to the FePt/TaO_x bilayer after annealing at 600 °C. The increase of the annealing temperatures led to larger grain sizes as indicated by the HRTEM image. The diffusion from TaO_x layer into FePt layer was proved by the cross-section TEM image and the XPS depth profile. On the other hand, the increasing annealing temperature also influenced the magnetic properties of FePt/TaO_x bilayer, leading to a higher coercivity in the in-plane direction. However, the coercivity of FePt/TaO_x bilayer after annealing at 550 °C in the out-of-plane direction exhibited the largest coercivity of 4.2 kOe, which was larger than FePt/TaO_x bilayer after annealing at either 600 °C or 650 °C. The above results show that suitable annealing temperature can increase the anisotropy of FePt with TaO_x capping layer and thus increase its magnetic coercivity.

Acknowledgments

This work was supported by the Seed Funding Program for Basic Research from the University of Hong Kong, the RGC-GRF grant (HKU 7049/11P), the RGC-GRF grant (PolyU 5013/08P), the Ministry of Economic Affairs of Taiwan (98-EC-17-A-08-S1-006) and National Science Council of Taiwan (NSC 99-2218-E-115-006-MY2).

Reference

[1] F. Akagi, M. Mukoh, M. Mochizuki, J. Ushiyama, T. Matsumoto, H. Miyamoto, J. Magn. Magn. Mater. 324 (2012) 309–313.
[2] Y. Inaba, K.L. Torres, A. Cole, R. Vanfleet, R. Ott, T. Klemmer, J.W. Harrell, G.B. Thompson, J. Magn. Magn. Mater. 321 (2009) 2451–2458.
[3] A. Perumal, Y.K. Takahashi, K. Hono, J. Appl. Phys. 105 (2009) 07B732.
[4] R.J. Tang, W.L. Zhang, Y.R. Li, J. Magn. Magn. Mater. 322 (2010) 3490–3494.
[5] M. Ghidini, A. Lodi-Rizzini, C. Pernechele, M. Solzi, R. Pellicelli, G. Zangari, P. Vavassori, J. Magn. Magn. Mater. 322 (2010) 1576–1580.
[6] Y.K. Takahashi, K. Hono, Appl. Phys. Lett. 84 (2004) 383–385.
[7] K. Aimuta, K. Nishimura, S. Hashi, M. Inoue, IEEE Trans. Magn. 41 (2005) 3898–3900.
[8] F. Albertini, L. Nasi, F. Casoli, S. Fabbrici, P. Luches, A. Rota, S. Valeri, J. Magn. Magn. Mater. 316 (2007) E158–E161.
[9] G.J. Li, C.W. Leung, Z.Q. Lei, K.W. Lin, P.T. Lai, P.W.T. Pong, Thin Solid Films 519 (2011) 8307–8311.
[10] F. Casoli, L. Nasi, F. Albertini, S. Fabbrici, C. Bocchi, F. Germini, P. Luches, A. Rota, S. Valeri, J. Appl. Phys. 103 (2008) 043912.
[11] T. Narisawa, T. Hasegawa, S. Ishio, H. Yamane, J. Appl. Phys. 109 (2011) 033918.
[12] Y.S. Yu, H.B. Li, W.L. Li, M. Liu, Y.M. Zhang, W.D. Fei, D.J. Sellmyer, Thin Solid Films 518 (2010) 2171–2174.
[13] N. Zotov, R. Hiergeist, A. Savan, A. Ludwig, Thin Solid Films 518 (2010) 4977–4985.
[14] J.S. Chen, J.P. Wang, J. Magn. Magn. Mater. 284 (2004) 423–429.
[15] D.H. Wei, Y.D. Yao, IEEE Trans. Magn. 45 (2009) 4092–4095.
[16] K.M. Yin, L. Chang, F.R. Chen, J.J. Kai, Mater. Chem. Phys. 71 (2001) 1–6.
[17] S.N. Song, Z.T. Song, L.C. Wu, B. Liu, S.L. Feng, J. Appl. Phys. 109 (2011) 034503.
[18] Y.K. Takahashi, T. Koyama, M. Ohnuma, T. Ohkubo, K. Hono, J. Appl. Phys. 95 (2004) 2690–2696.
[19] S.N. Hsiao, F.T. Yuan, H.W. Chang, H.W. Huang, S.K. Chen, H.Y. Lee, Appl. Phys. Lett. 94 (2009) 07A737.
[20] H.-U. Hummel, R. Fackler, P. Remmert, Chem. Ber. 125 (1992) 551–556.
[21] Y.F. Ding, J.S. Chen, E. Liu, C.J. Sun, G.M. Chow, J. Appl. Phys. 97 (2005).
[22] Y.F. Xu, J.S. Chen, J.P. Wang, Appl. Phys. Lett. 80 (2002) 3325–3327.
[23] Y.F. Xu, J.S. Chen, D.Y. Dai, J.P. Wang, IEEE Trans. Magn. 38 (2002) 2042–2044.